Available online at www.sciencedirect.com
SCIENCE DIRECT®
ELSEVIER
International Journal of Multiphase Flow 29 (2003) 1771–1792
International Journal of Multiphase Flow
www.elsevier.com/locate/ijmulflow

Forced convective boiling heat transfer in microtubes at low mass and heat fluxes

Tzu-Hsiang Yen, Nobuhide Kasagi *, Yuji Suzuki

Department of Mechanical Engineering, The University of Tokyo, Bunkyo-ku, Hongo 7-3-1, Tokyo 113-8656, Japan

Received 21 May 2003; received in revised form 10 September 2003

Abstract

Convective boiling of HCFC123 and FC72 in 0.19, 0.3 and 0.51 mm ID tubes is investigated. The experimental setup as well as the data reduction procedure has carefully been designed, so that the relative uncertainty interval of the measured heat transfer coefficient in microtubes is kept within ±10%. Up to 70 K liquid superheat over the saturation temperature is observed at low heat and mass fluxes. The onset of the superheat is found to be dependent on the mass flux and the boiling number of the refrigerant examined. In the saturated boiling regime, the heat transfer characteristics are much different from those in conventional-size tubes. The heat transfer coefficient is monotonically decreased with increasing the vapor quality, and becomes independent of the mass flux. Most empirical formulas are not in accordance with the present experimental data. Since the prediction using the nucleate boiling term of Kandlikar's empirical correlations coincides with the present results, the convection effect should be minor in microtubes. On the other hand, the pressure loss characteristics are qualitatively in accordance with the conventional correlation formula while quantitatively much lower. These phenomena can be explained by the fact that the annular flow prevails in microtubes.

1. Introduction

Highly efficient heat exchangers have become even more important because of the rapid increase of the heat dissipation rate in high-end electronic devices. Since Tuckerman and Pease (1981) obtained large overall heat transfer coefficient in microchannels fabricated on a Si wafer,

* Corresponding author. Tel.: +81-3-5841-6417; fax: +81-3-5800-6999.
E-mail address: kasagi@thtlab.t.u-tokyo.ac.jp (N. Kasagi).

0301-9322/$ - see front matter © 2003 Elsevier Ltd. All rights reserved.
doi:10.1016/j.ijmultiphaseflow.2003.09.004

heat transfer research in microconduits for both single and multi-phase flows have attracted much attention.

Paitoonsurikarn et al. (2000) proposed compact micro-bare-tube heat exchangers, in which a tube bank of small diameter tubes was employed without any extended heat transfer surface. They developed a new optimal design method based on simulated annealing, and found that the efficiency is markedly improved over commercial louver-finned heat exchangers for both single and two-phase flows. The optimum tube inner diameter is 0.3–0.5 mm, and the optimum heat and mass fluxes are relatively small. In their optimal design procedure for evaporators, however, they used empirical correlations of convective boiling in larger diameter tubes (>2 mm) for estimating the heat transfer coefficient and pressure loss. Because the convective boiling characteristics in microtubes are known to be much different from those in conventional (>3 mm) or small size (0.6–3 mm) tubes (Kandlikar, 2002), the above optimization may lead to an inappropriate design.

In the last decade, peculiar heat transfer characteristics of convective boiling have been reported in minitubes (0.6–3 mm) and microtubes (<0.6 mm, e.g., Kandlikar, 2002; Mehendale et al., 2000). In minitubes, recent convective boiling experiments (Bao et al., 2000; Wambsganss et al., 1993; Kew and Cornwell, 1997) show that the heat transfer coefficient weakly depends on the mass flux and the vapor quality, while strongly on the heat flux and the system pressure. It is also found that nucleate boiling is the dominant heat transfer mechanism whilst the contribution of the convective boiling is minor. This fact indicates that the heat transfer mechanism in minitubes is totally different from that in conventional tubes, in which the heat transfer coefficient is known to be dependent on the vapor quality, and the mass and heat fluxes (e.g., Zurcher et al., 1999). On the other hand, Hapke et al. (2000) carried out convective boiling experiments in a 1.5 mm ID tube and found that the onset of boiling occurred at a higher liquid superheat temperature than that in the conventional tubes.

In microtubes, high liquid superheat phenomena were also discovered. Peng and Wang (1993) carried out convective subcooled boiling experiments in 200–600 μm ID microchannels and reported that nucleation bubbles were hardly observed in the boiling regime. They called this phenomenon 'bubble extinction'. They also found that the nucleate boiling in their microchannels started only when liquid superheat became sufficiently large. They proposed theoretical models, which were based on the Clausius–Claypeyron equations and statistical thermal dynamics to predict the measured superheat temperature. However, their model did not take into account the effect of the surface chemistry or surface cavities, which had been proved as an important parameter in nucleate boiling (Carey, 1992).

Recently, such high liquid superheat was attributed to the lack of active nucleate sites. Zhang et al. (2002) conducted a series of experiments in microchannels of 28–171 μm ID. They showed that the wall superheat temperature before the onset of nucleate boiling was about 5 K lower on surfaces with microcavities than that on smooth wall. Brereton et al. (1998) employed a heterogeneous nucleation theory with the empirical correlation of active nucleation sites in order to predict the nucleation temperature inside capillary tubes. Two research groups above reported that the reduction of active nucleation cavities and vapor nuclei in microconduits should be responsible for the unusually high liquid superheat. However, the dominant parameters for the onset and the magnitude of the superheat are still unknown.

Since accurate measurement of temperature, pressure, heat flux and mass flow rate in a single microtube is extremely difficult, detailed heat transfer data in microtubes of less than 1 mm ID are

still lacking. Bowers and Mudawar (1994) measured CHF temperature and wall temperature in their mini and micro channel test sections. Ravigururajan (1998) measured the average heat transfer coefficient in parallel microchannels of 425 μm ID. To the authors' knowledge, only Saitoh et al. (2000), who employed 1.12 and 0.51 mm ID tubes with R-134a refrigerant, offer the local heat transfer coefficient data.

The objectives of the present study are, (1) to clarify the condition for the onset of liquid superheat, which deteriorates heat transfer, and (2) to obtain local heat transfer coefficients and pressure losses of convective boiling in microtubes. We carried out a series of experiments on saturated convective boiling in microtubes of 0.19, 0.3 and 0.51 mm ID at low heat (1–13 kW/m^2) and mass (50–300 kg/m^2 s) fluxes. These experimental conditions were chosen after the optimal design of compact evaporators (Paitoonsurikarn et al., 2000).

2. Experimental apparatus and procedure

Figs. 1 and 2 show the flow loop and the test section used in the present experiments in microtubes. Two different refrigerants, i.e., HCFC123 and FC72, were employed as a working fluid. A twin plunge pump (Moleh, MT-2221) was employed in most experiments carried out in order to provide mass flux from 50 to 300 kg/m^2 s. Unlike a single plunge pump, the twin plunge pump keeps a constant flow rate without introducing unwanted bubbles into the test section. The uncertainty interval of the flow rate is within ±1%. The working fluid was heated with a secondary water loop at the inlet, and its temperature was kept at 10 K below the saturated temperature.

SUS304 stainless steel tubes, covered with glass cotton for thermal insulation, were employed as a test section of 280 mm in length. The inner diameter was chosen as 0.19, 0.3 and 0.51 mm, while the outer diameter is 0.41, 0.55 and 0.81 mm, respectively. The tolerance of the inner diameter of the test section is ±20 μm, while that of the outer diameter is respectively ±10, ±10 and ±20 μm for 0.19, 0.3 and 0.51 mm ID tubes. Direct measurements of the outer diameters of the 0.19 and 0.51 mm microtubes show that their accuracy are all in the range of the tolerance. The error in the length of the microtube is ±1 mm. The microtube and the inlet/outlet block were fixed by soldering. Thus, there is a sudden contraction and expansion at the inlet and outlet of the test section, respectively.

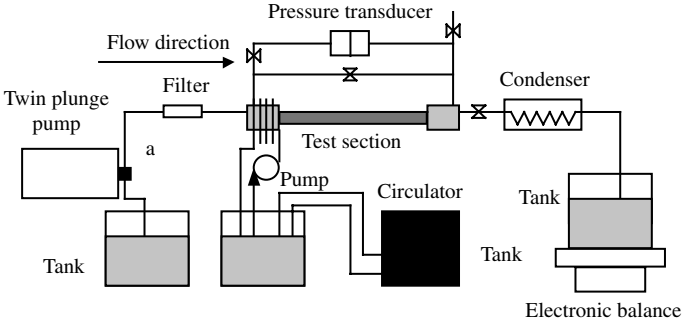

Fig. 1. Experimental loop.

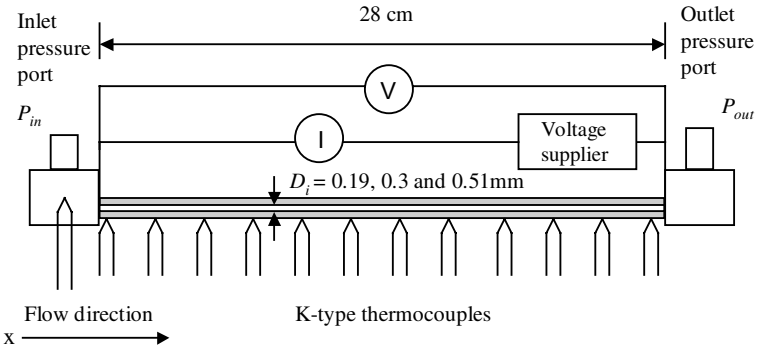

Fig. 2. Test section.

The test section was heated by a direct current, and the heat loss to the environment was compensated as described later. Twelve K-type thermocouples of 25 μm OD were glued onto the tube outer wall with thermally conductive silicon ($k = 0.9$ W/(mK), Shin-Etsu Silicones, KE3493). A magnified view of a thermal couple and the test section without thermally conductive silicon is shown in Fig. 3. One K-type thermocouple was inserted into the inlet manifold for the measurement of the inlet fluid temperature. Cold junctions of the thermocouples were submerged into a standard temperature bath (Komatsu Electronics, Model ZC-114), in which the temperature was maintained at 0–0.02 °C. Calibration of the thermocouples was made between 20 and 85 °C. Standard estimation errors of the thermocouples were within ±0.1 K.

In the case of 0.3 mm ID tube experiment, however, a syringe pump and thermocouples with an accuracy of ±0.2 K were employed. Since the flow driven by the syringe pump was repeatedly started with a duration of 150–600 s and made the heat transfer measurement somewhat unstable, we mainly focus on the experimental data for 0.19 and 0.51 mm ID tubes.

The pressure loss of the test section was measured by a diaphragm pressure transducer (Sokken, PZ-77-D) through the inlet and outlet pressure ports. The uncertainty of the pressure transducer is within ±0.1 kPa. The absolute inlet pressure was also measured with the same pressure transducer by opening one side of the diaphragm to the atmosphere through the valve shown in Fig. 1. We

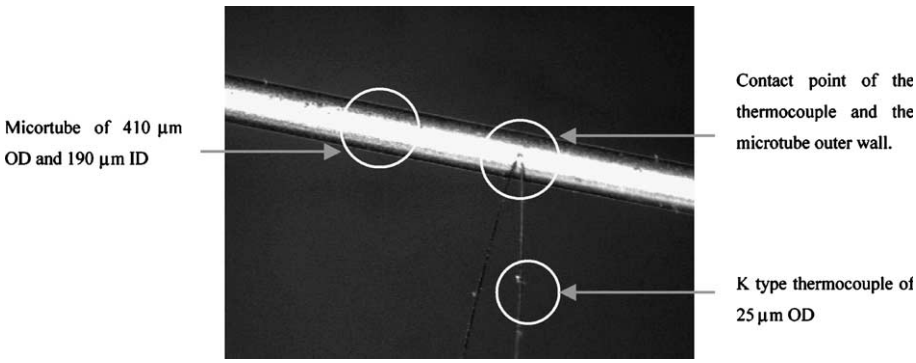

Fig. 3. The connection of the thermocouple of 25 μm OD and the test section of 0.51 mm OD.

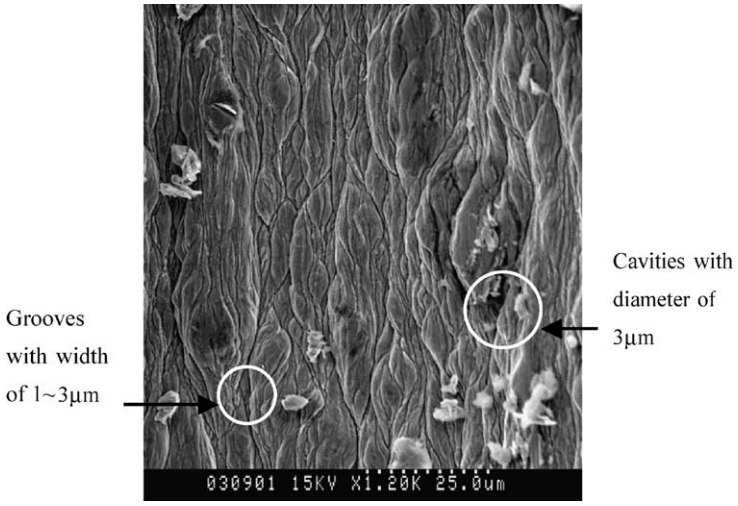

Fig. 4. SEM image of inner wall of the test section (0.19 mm ID).

define a steady state in such a way that the pressure fluctuation falls below ±0.1 and ±0.5 kPa for 0.19 and 0.51 mm ID tubes, respectively. It usually takes one hour to reach this state during each run.

Since the present experimental setup is an open loop, the exit of the test section is maintained at 1atm. Thus, the total system pressure is determined by the pressure loss of the test section. It is about 110–125 kPa at 0.51 mm and 135–145 kPa at 0.19 mm ID.

Fig. 4 shows an SEM image of the inner surface of the 0.19 mm ID tube. Grooves with 1–3 μm width and cavities having diameters of about 3–4 μm are distributed. Similar surface structures are also found in the 0.3 and 0.51 mm ID tubes.

3. Data reduction

The heat flux transferred to the working fluid q (W/m^2) is calculated as

$$q(x) = I^2R(x)/\pi D_i - q_{\text{loss}}(x), \tag{1}$$

where $I^2R(x)$ corresponds to the Joule heating. The local heat loss from the test section to the environment $q_{\text{loss}}(x)$, depends on the outer wall temperature $T_{\text{w out}}$ and the environmental temperature T_{air}, and is given by

$$q_{\text{loss}}(x) = h_{\text{loss}}(T_{\text{w out}}(x))(T_{\text{w out}}(x) - T_{\text{air}}). \tag{2}$$

Since T_{air} is almost constant, h_{loss} is assumed to be a function of $T_{\text{w out}}$, and determined through a preliminary heating experiment with keeping the test section empty. In the actual convective boiling experiment, the maximum heat loss is less than 20% of the total heat generation.

The electric resistance of the test section per unit length $R(x)$ should vary with the outer wall temperature as

$$R(x) = R_0(1 + \alpha T_{w\,out}), \tag{3}$$

where α is TCR (temperature coefficient of resistance) of the test section. The measured value of TCR is 8.35×10^{-4} (1/K), and in good agreement with the TCR of the SUS304 stainless steel.

Since the axial heat conduction is negligible, the inner wall temperature T_{win} is calculated by solving the one-dimensional heat conduction equation in the cylindrical coordinates. With the boundary conditions at the outer wall, i.e.,

$$-k\left(\frac{\partial T}{\partial r}\right)_{r=D_0/2} = q_{loss} \tag{4}$$

and

$$T|_{r=D_0/2} = T_{w\,out}, \tag{5}$$

we obtain

$$T_{w\,in} = T_{w\,out} + \left(\frac{q(x)\pi D_i}{4k}\right)\left[\frac{\left(\frac{D_0}{D_i}\right)^2\left(1 - \ln\left(\frac{D_0}{D_i}\right)^2\right) - 1}{1 - \left(\frac{D_0}{D_i}\right)^2}\right]. \tag{6}$$

The heat transfer coefficient is calculated as

$$h(x) = \frac{q}{T_{w\,in}(x) - T_{ref}(x)}, \tag{7}$$

where $T_{ref}(x)$ is the local bulk mean temperature of the refrigerant. When the fluid is in the saturated region, the local bulk mean temperature is equal to the saturation temperature, and is derived from the local pressure distribution $P_{sat}(x)$ described below.

The thermal entrance length (Kays and Crawford, 1993) is within 8 mm under all experimental conditions. Therefore, the thermal entrance region only exists in the subcooled region and its effect on the convective boiling can be neglected.

The total pressure loss ΔP_{total} in the test section can be decomposed as

$$\Delta P_{total} = \Delta P_{sub} + \Delta P_{sat} + \Delta P_{sup}, \tag{8}$$

where ΔP_{sub}, ΔP_{sat}, and ΔP_{sup} are the pressure losses in the subcooled liquid, saturated boiling and superheated vapor regions, respectively. The length of the subcooled region l and the pressure loss ΔP_{sub} are calculated as follows. We first assume an arbitrary value for l, and calculate ΔP_{sub} as

$$\Delta P_{sub} = f\frac{1}{2}\rho U^2\frac{l}{D_i}, \tag{9}$$

where f, ρ and U are the friction factor of the laminar Poiseuille flow, the liquid density and the bulk mean velocity, respectively. The saturation pressure at $x = l$ is given by

$$P_{sat}(l) = P_{in} - \Delta P_{sub}, \tag{10}$$

where P_{in} is the inlet pressure. Then, the saturation temperature T_{sat} is calculated from the saturation table of the refrigerant (REFPROP). Finally, the new value of l is obtained from the energy balance, i.e.,

$$\int_0^l q(x)\pi D_i \,\mathrm{d}x = \dot{M} C_p (T_{\mathrm{sat}}(l) - T_{\mathrm{in}}). \tag{11}$$

The iterative calculation using Eqs. (9)–(11) is repeated until the value of l converges.

The local vapor quality χ in the saturated region is calculated as

$$\chi(x) = \frac{\int_l^x q(x)\pi D_i \,\mathrm{d}x}{\dot{M} h_{lv}}. \tag{12}$$

The length of the saturated region s is determined from the above integration in such a way that $\chi = 1$ at $x = l + s$. The pressure loss in the superheat region ΔP_{sup} ($l + s < x \leqslant L$) is determined by the laminar flow solution for vapor using physical properties at the local pressure and temperature.

Finally, the pressure loss in the saturated boiling region, ΔP_{sup}, is determined by Eq. (9). The local pressure $P_{\mathrm{sat}}(x)$ in the saturated boiling region is assumed to be linearly distributed along the tube, and given by

$$P_{\mathrm{sat}}(x) = P_{\mathrm{sat}}(l) - \Delta P_{\mathrm{sat}} \frac{x - l}{s}. \tag{13}$$

After the pressure loss of the test section reaches the steady state as defined in Section 2, the wall temperature shows some quasi-periodic variation in the saturated boiling conditions. The period is about 20 s and the amplitude is 0.3 and 0.8 K in 0.19 and 0.51 mm ID tubes, respectively. Such temperature variation may be due to the bubble generation inside the tube. The average wall temperature is obtained by ensemble averaging over 30 min.

The propagation of the componential uncertainties through data reduction is estimated by ANSI/ASME PTC 19.1. The uncertainty interval of the inner wall temperature at 95% coverage is about 0.13 °C. Those of the heat flux and the heat transfer coefficient are within ±5% and ±10%, respectively.

4. Experimental results

4.1. Single-phase heat transfer and pressure loss

In order to assess the present pressure and heat transfer measurements, a single-phase flow experiment was made. As shown in Fig. 5, the friction factor presently measured in microtubes is in good agreement with its analytical laminar flow value in the Reynolds number range examined. Fig. 6 shows the distribution of the Nusselt number along the tube length. There is a small scatter, but the data are also in reasonable agreement with the analytical value for laminar heat transfer with constant wall heat flux. Note that the heat flux in the convective boiling experiment described later is much larger than that used in the single-phase flow measurement. Therefore, the error in the heat loss compensation is smaller, so that the data scatter should be much less in the flow boiling cases.

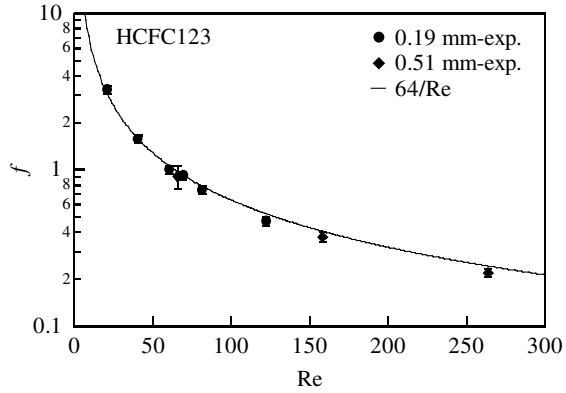

Fig. 5. Friction factor in single phase laminar flow.

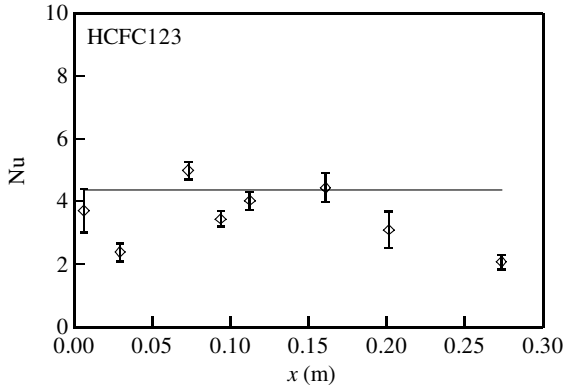

Fig. 6. Nusselt number in single-phase laminar flow (0.3 mm ID).

4.2. Wall temperature

Fig. 7 shows the distribution of the absolute wall temperature in the 0.19 mm ID tube at $\dot{m} = 145$ kg/m^2 s. When $q = 5.5$ kW/m^2, the wall temperature measured is in accordance with the saturated temperature between $x = 0.04$ and 0.20 m. It decreases with increasing x due to the pressure drop in the test section. Thus, conventional saturated boiling should occur under this heat flux condition. On the other hand, the wall temperature for a smaller heat flux ($q = 2.4$ kW/m^2) monotonically increases with the axial distance, and reaches 110 °C at $x = 0.27$ m.

Fig. 8 shows the temperature distribution in the 0.51 mm ID tube. When $q = 2.8$ kW/m^2, the wall temperature increases with x and reaches a maximum value of 45 °C at $x = 0.15$ m. Then, it suddenly drops to the saturated temperature downstream, and saturated boiling occurs at $x > 0.15$ m. On the other hand, normal saturated boiling is observed with a higher heat flux of $q = 12.6$ kW/m^2.

Fig. 9 shows the Nusselt number distribution in the 0.51 mm ID tube when the wall temperature exceeds the saturation temperature. The Nusselt number is in accordance with the laminar

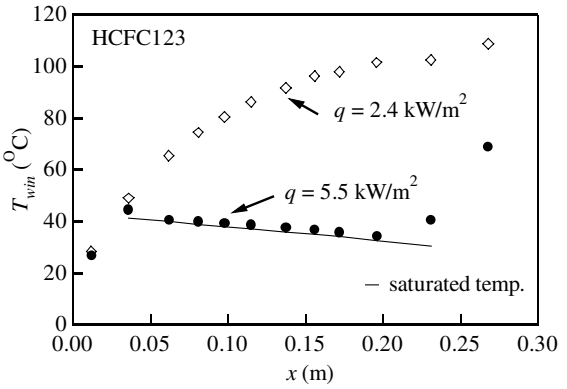

Fig. 7. Wall temperature distribution in 0.19 mm ID tube at $\dot{m} = 145$ kg/m^2 s.

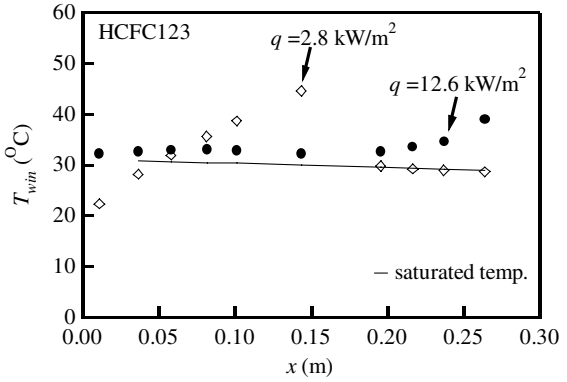

Fig. 8. Wall temperature distribution in 0.51 mm ID tube at $\dot{m} = 145$ kg/m^2 s.

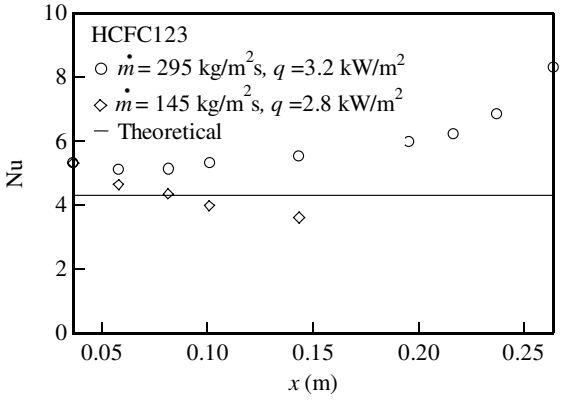

Fig. 9. Nusselt number under the liquid superheat condition in 0.51 mm ID tube.

flow value with the constant heat flux ($Nu = 4.316$) at $x < 0.15$ m. The pressure drop is also in good agreement with the estimates based on the single-phase laminar flow (not shown here). These facts indicate that liquid superheat phenomena, which is also observed for a stagnant fluid in capillaries by Brereton et al. (1998), should also occur in the present experiment. The Nusselt number in Fig. 9 starts to deviate from the theoretical value at $x > 0.15$ m. This is probably because the physical properties of the fluid are not the same as those of the saturated liquid.

4.3. Dominant parameters for the superheat phenomena

Fig. 10 shows the condition map for the superheat phenomena as a function of the boiling number *Bo* and the mass flux $\dot{m}$. When $\dot{m}$ is fixed, the superheat occurs at small *Bo*. On the other hand, when the mass flux increases, the critical *Bo* for the onset of boiling decreases and seems to be independent of the tube inner diameter. Fig. 11 shows the map for FC72 and HCFC123 in the 0.19 mm ID tube. The superheat regime is almost the same for the two different refrigerants, which have different latent heats, but similar surface tension.

The fact that the superheat only occurs at low *Bo* implies that there exists some threshold of the heat flux for making the nucleation cavities in microtubes active. The radius r_c of active cavity (Hsu, 1969) is given by

$$r_c = \frac{\delta}{2C_1}\left[\left(1 - \frac{\Delta T_{sat}}{\Delta T_w}\right) \pm \sqrt{\left(1 - \frac{\Delta T_{sat}}{\Delta T_w}\right)^2 - \frac{4AC_2}{\delta \Delta T_w}}\right], \tag{14}$$

where δ is the thermal layer thickness. Quantities C_1 and C_2 are constant values, which are dependent on the contact angle of the refrigerant, and A is the physical parameter representing $2\sigma T_{sat}/h_{lg}\rho_g$. Temperature differences ΔT_{sat} and ΔT_w are defined as

$$\Delta T_{sat} = T_{ref} - T_{sat} \tag{15}$$

and

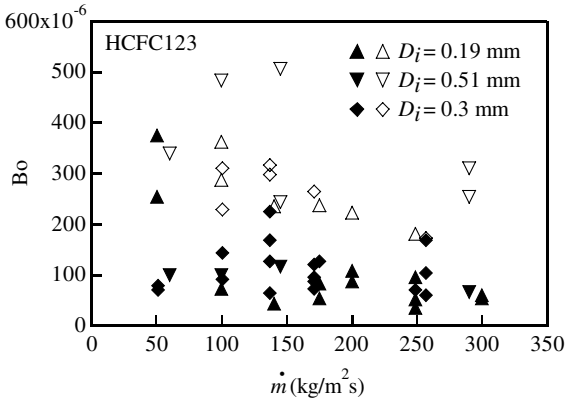

Fig. 10. Onset of liquid superheat in different inner diameter tubes for HCFC123. Open symbols represent saturated boiling, while close symbols superheat liquid.

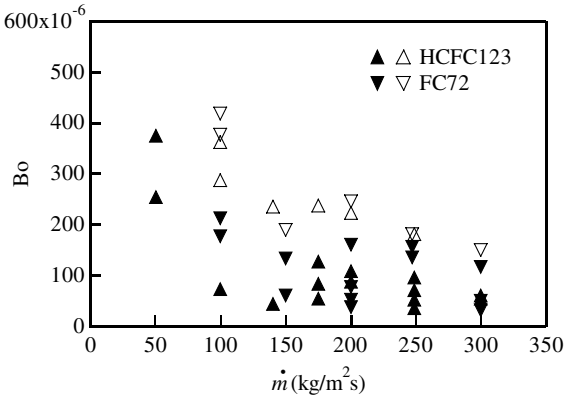

Fig. 11. Onset of liquid superheat for different refrigerants in 0.19 mm ID tube. Open symbol represents the saturated boiling region, while close symbol the superheat region.

$$\Delta T_{\mathrm{w}} = T_{\mathrm{w\,in}} - T_{\mathrm{ref}}. \tag{16}$$

By assuming that r_{c} and δ are respectively equal to the radius of cavities shown in Fig. 3 ($\sim$3 μm) and the radius of the 0.19 mm ID tube, ΔT_{w} should be larger than 2.5 K to activate the nucleation site. On the other hand, when $Bo = 0.00035$ and $\dot{m} = 70$ kg/m^2 s, of which condition is close to the boundary between the superheat and saturated boiling regions shown in Fig. 9, ΔT_{w} determined from the heat flux and the Nusselt number for the laminar flow is 2.5–4.8 K and in accordance with the Hsu's classical theory. However, the classical active nucleation theory is not sufficient to explore the superheat mechanism, since Eq. (15) does not include the mass flux, which also affects the onset of the superheat and thus changes ΔT_{w} in the present experiment.

Fig. 12 shows the maximum superheat temperature for different tube diameters at various heat and mass fluxes. Although the superheat temperature varies in a wide range, its maximum value is 100 and 45 °C for the 0.19 and 0.51 mm ID tubes, respectively. Fig. 13 shows the wall temperature distribution for different heat fluxes in the same experimental run. The superheat temperature

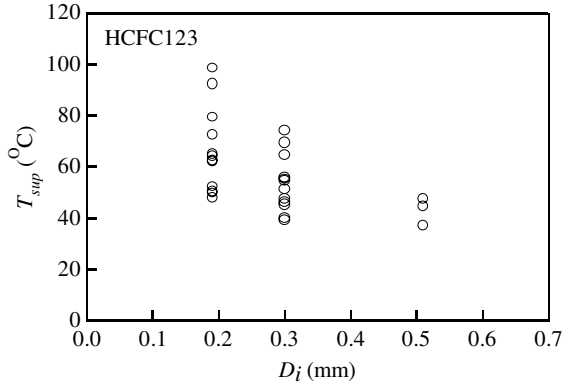

Fig. 12. Superheat temperature versus inner diameter.

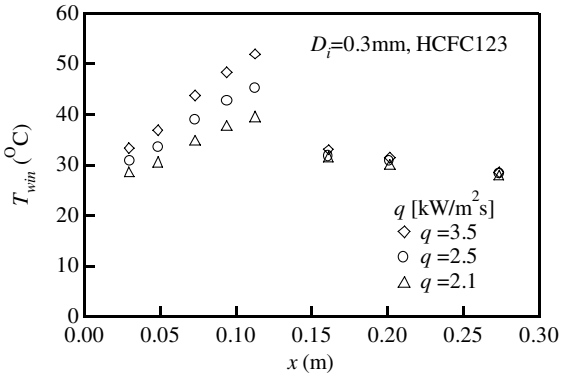

Fig. 13. Temperature distribution under different heat fluxes in the same experimental run at $\dot{m} = 170$ kg/m^2 s.

increases with the heat flux, but the saturated boiling begins at the same axial position. Thus, once the nucleate boiling starts, it occurs at the same axial position of the test section, i.e., probably at the same nucleate site. The location of nucleation site often changes when the working fluid flow stops and restarts between successive runs. From this observation, it is conjectured that the size of the active cavity and the presence of entrapped gas in the cavity should be crucial for determining the maximum superheat temperature and this is the cause of large scatter of the superheat temperature shown in Fig. 13.

Brereton et al. (1998) employed a heterogeneous boiling theory together with empirical correlations for the number density of the active sites in pool boiling, and proposed a formula for predicting the nucleation temperature in microcapillaries. In their final form, the growth rate of the vapor embryos per unit area J is given by

$$J = \alpha\left(\frac{r_{\text{avg}}}{r_{\text{crit}}}\right)^{b} n_{\text{surface}}\sqrt{\frac{3\sigma}{\pi m}}\exp\{-W_{\max}/(kT_{\text{sup}})\}, \tag{17}$$

where r_{avg} is the average cavity radius, r_{crit} is the critical radius for a nucleate bubble to grow, and σ is the surface tension of the liquid. The quantities m, $W_{\max}$ and T_{sup} are the molecular weight, the work required for a bubble to grow to the critical radius, and the liquid superheat temperature, respectively. The factor of $\alpha(\frac{r_{\text{avg}}}{r_{\text{crit}}})^{b}$ is the empirical function, which is derived form pool boiling experiments, representing the number density of active nucleate sites. The number of molecules on the wall n_{surface} can be given by

$$n_{\text{surface}} = \frac{\pi D_i}{s_{\text{m}}}, \tag{18}$$

where s_{m} is the mean distance between molecules. The threshold of J for the nucleate boiling is 10^{18}–10^{20} (1/m^2 s). Fig. 14 shows T_{sup} given by Eq. (17) versus D_i. The maximum superheat temperature presently observed is in accordance with the prediction when D_i is small, while it deviates for larger D_i. This fact indicates that the maximum superheat temperature increases with decreasing the tube diameter, because the confined space limits the number of active sites. Note that the spinodal superheat limit becomes higher than T_{sup} given by Eq. (17) at $D_i < 0.1$ mm.

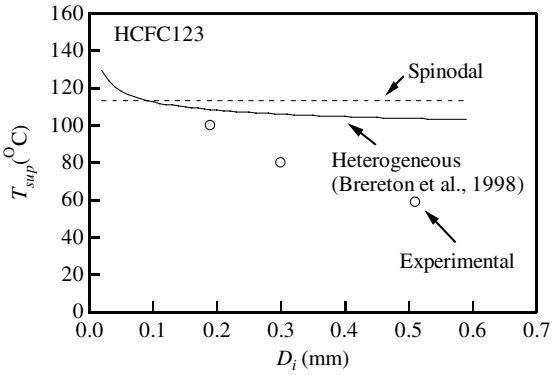

Fig. 14. The maximum superheat temperature versus inner diameter.

Figs. 15 and 16 show the superheat temperature as functions of the mass and heat fluxes in the 0.3 mm ID tube, respectively. It is found that the superheat temperature is almost independent of the mass and heat fluxes, and this is in accordance with the Brereton's theoretical formula given by Eq. (17).

It is now clear that there are two parameter groups contributing to the superheat phenomena presently observed. The maximum superheat temperature depends on the tube diameter and the cavity distribution on the tube wall, while the onset of superheat for a specified tube diameter is ruled by the boiling number and the mass flux.

4.4. Heat transfer characteristics for saturated boiling

The heat transfer characteristics in the case of conventional saturated boiling are discussed in this section. Typical distributions of the heat transfer coefficient against the vapor quality are shown in Fig. 17. The heat transfer coefficient h decreases from 8000 to 4000 W/m^2 K as the vapor quality χ is increased to $\chi = 0.3$, then remains constant at 2000–4000 W/m^2 K toward $\chi = 1$. Such

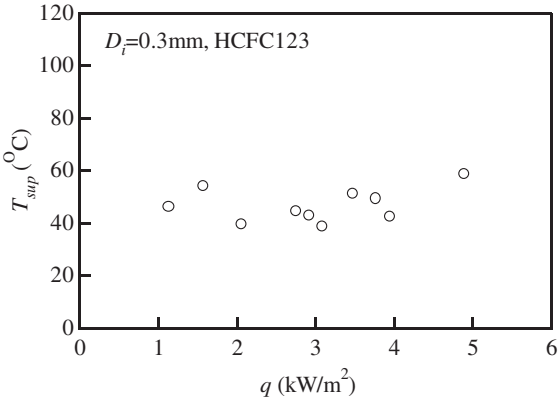

Fig. 15. Superheat temperature versus heat flux.

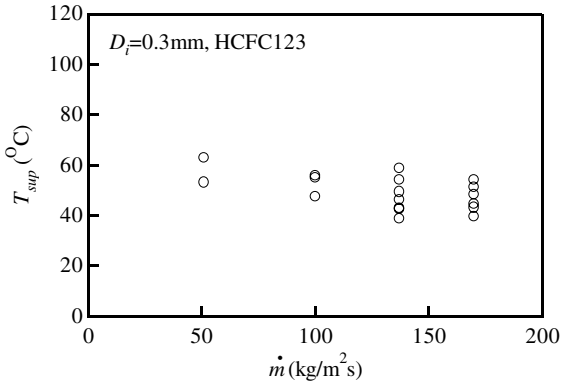

Fig. 16. Superheat temperature versus mass flux.

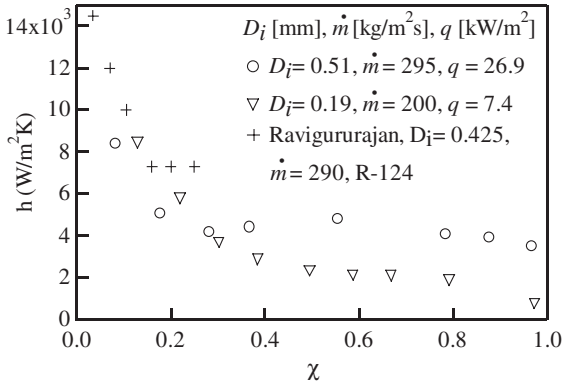

Fig. 17. Typical heat transfer coefficient distribution.

variation of the heat transfer coefficient is completely different from those in small or traditional-size tubes, where the convective boiling effect is dominant and the heat transfer coefficient increases with increasing χ at $\chi < 0.9$.

Ravigururajan (1998) also reported similar experimental results in the microchannels of a hydraulic diameter of 425 μm at similar mass fluxes as shown in Fig. 17. Saitoh et al. (2000) also found that the heat transfer coefficient decreases with increasing χ in their 0.51 mm ID tube.

Heat transfer coefficients at different heat fluxes in the 0.51 mm ID tube are shown in Fig. 18. Again, h for all the experimental condition decreases with increasing χ at $\chi < 0.3$, and remains a constant for larger χ. When the heat flux q is increased, h is decreased for $q < 14.9$ kW/m^2 and then approaches an asymptotic curve. This phenomenon is opposite to that observed in traditional or small-size tubes, where h is increased with increasing q. Fig. 19 shows the heat transfer coefficient for different mass fluxes $\dot{m}$. Since h is independent of $\dot{m}$, the convective boiling effect should be minor.

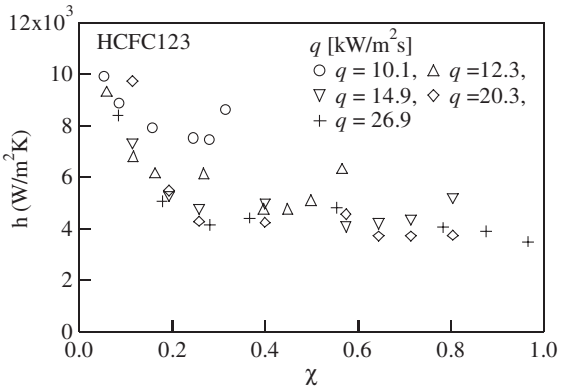

Fig. 18. Heat transfer coefficient versus quality at different heat flux in 0.51 mm ID tube at $\dot{m} = 295$ kg/m^2 s.

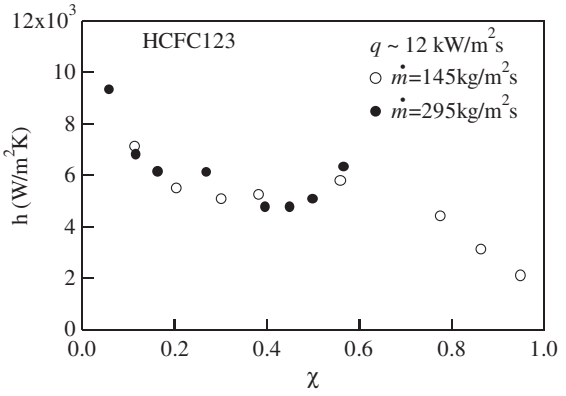

Fig. 19. Heat transfer coefficient versus quality at different mass flux in 0.51 mm ID tube at $q = 12$ kW/m^2 s.

It is conjectured that the heat transfer characteristics presently obtained in microtubes is caused by the size of nucleate bubble limited in the confined space. When bubbles grow, they immediately attach to the surrounding wall of the microtube. Thus, the heat transfer coefficient is suppressed under higher heat flux or mass flux conditions because of the limited evaporating space.

Fig. 20 shows comparison of our experimental results with empirical correlations by Liu and Winterton (1991), Shah (1976), Bjorge et al. (1982), Kandlikar (1990), Schrock and Grossman (1959) and Chen (1966), which were designed for larger tubes. It is found that most empirical correlations underpredict/overpredict the present data by more than an order of magnitude, except some nucleate boiling terms from Kandlikar's and Liu and Winterton's empirical correlations.

Kandlikar (1990) proposed an empirical correlation for microtubes given by

$$h = h_l[C_1 Co^{C_2}(25Fr)^{C_5} + C_3 Bo^{C_4} F_k], \tag{19}$$

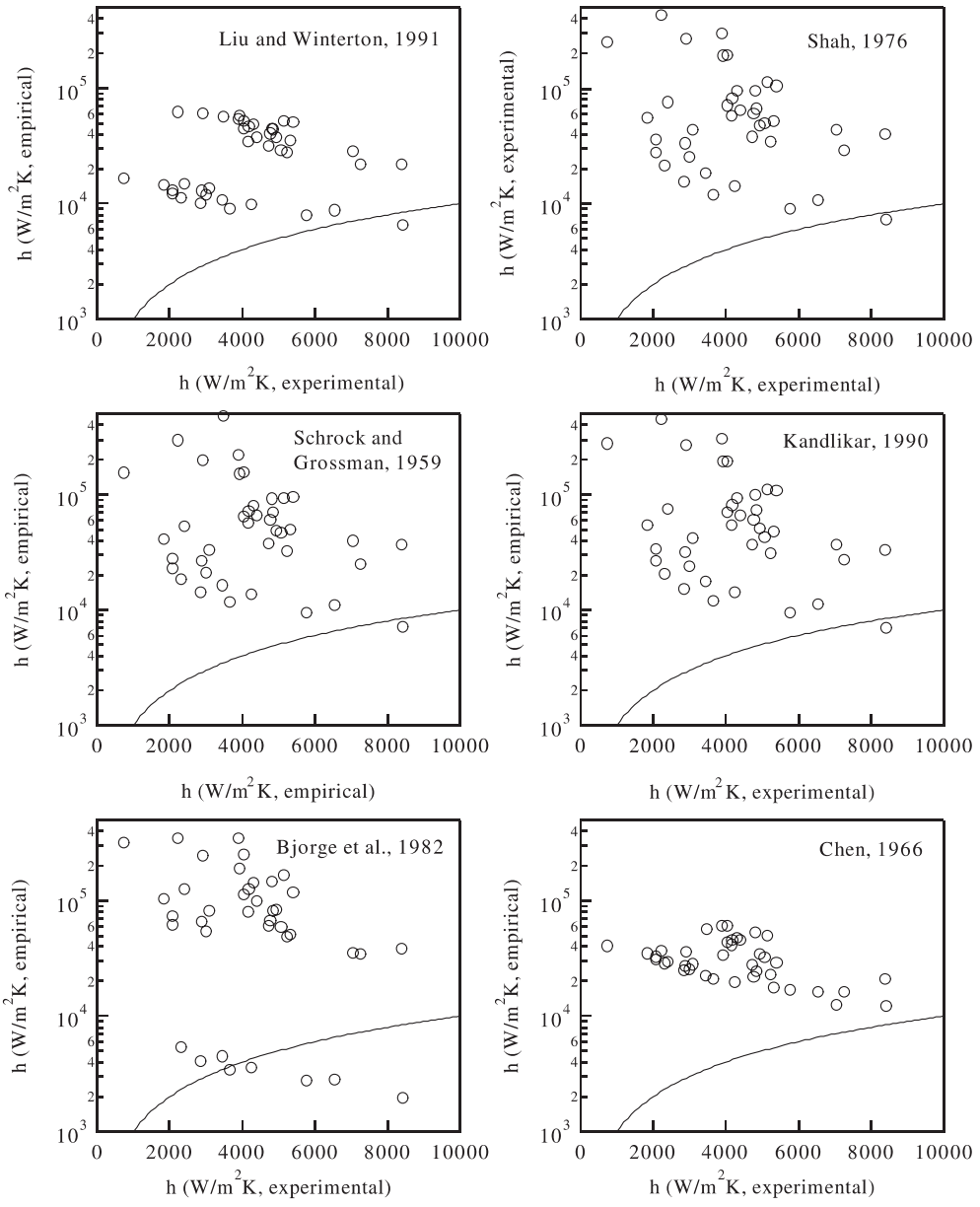

Fig. 20. Comparison of the experimental results of HCFC123 in 0.19 and 0.51 mm tubes with empirical correlations. Black lines represent the coincidence between the experimental data and the empirical function.

where h_l represents the single-phase heat transfer coefficient under the same heat and mass flux conditions, *Fr* is the Froude number, and *Co* is the convection number representing the effect of vapor quality and its relevant flow pattern defined by

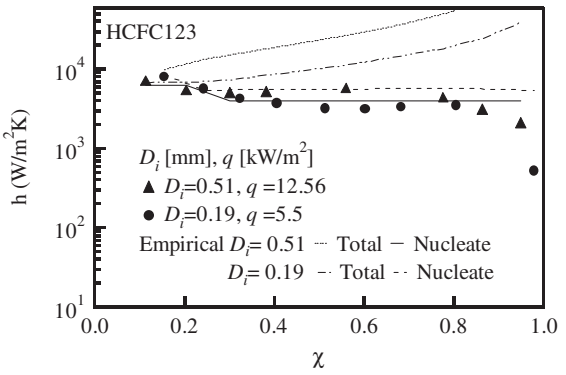

Fig. 21. Heat transfer coefficients for different tube diameters and their comparison with the Kandlikar's empirical correlation.

$$Co = \left(\frac{1-x}{x}\right)^{0.8}\left(\frac{\rho_v}{\rho_l}\right)^{0.5}. \tag{20}$$

The quantity of F_k in Eq. (19) is a parameter dependent on physical properties of the working fluid. Since F_k for HCFC123 is unavailable in the literature, we employ that of R-22, which has similar physical properties except vapor density and liquid viscosity. The numerical constants C_1–C_5 are functions of Co. The second term of Eq. (19) represents the nucleate boiling effect.

Fig. 21 shows the heat transfer coefficient given by the second term of Eq. (20) in comparison with the present experimental data. The Kandlikar's empirical correlation overpredicts the data especially for large χ. On the other hand, the nucleate boiling term in Eq. (19) is in accordance with the present data. Therefore, the convective boiling term, where the Froude number is the dominant parameter, has minor contribution in microtubes. The prediction with the nucleate boiling term is closer to the experimental results for the 0.19 mm ID tube than for the 0.51 mm ID tube, as the contribution of the nucleate boiling prevails as the inner diameter of microtube decreases.

4.5. Pressure losses

Fig. 22 shows the pressure loss in the saturated boiling region ΔP_{sat} versus the mass flux. The heat flux is chosen sufficiently large to keep the exit quality being unity. Fig. 23 shows the relationship between the exit vapor quality and the saturated pressure loss in the 0.51 mm ID tube. Tran et al. (2000) proposed an empirical function based on their experimental data for 2.46 and 2.92 mm ID tubes. In their formula, the pressure drop is given by

$$\Delta P = \bar{\phi}_{fl}^2 \times \Delta P_{fl}, \tag{21}$$

where ΔP_{fl} is the single phase pressure loss, and $\bar{\phi}_{fl}^2$ is

$$\phi_{fl}^2 = 1 + (C\Gamma^2 - 1)[N_{\text{conf}}\chi^{0.875}(1-\chi)^{0.875} + \chi^{1.75}]. \tag{22}$$

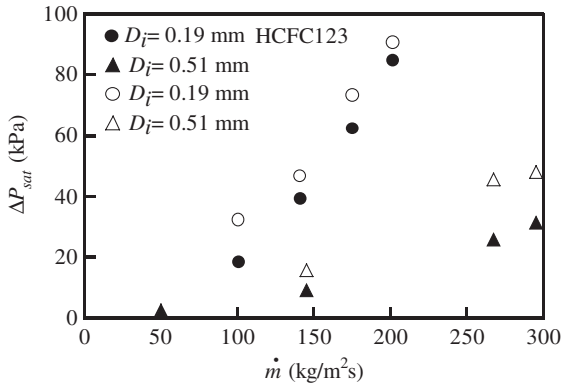

Fig. 22. Pressure loss versus mass flux of the saturated boiling region when χ reaches 1. Open and closed symbols represent empirical predictions and experimental results, respectively.

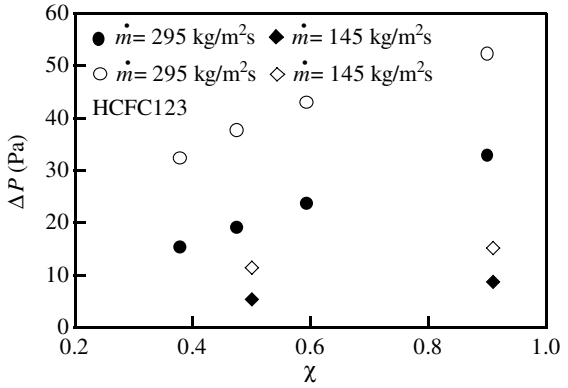

Fig. 23. Pressure loss versus vapor quality in 0.51 mm ID. Open and closed symbols represent empirical predictions and experimental results, respectively.

In Eq. (22), Γ^2 is the ratio of pressure losses for gas and liquid single phase flows. The quantity N_{conf} is the confined number proposed by Kew and Cornwell (1997) to describe characteristics in minitubes of ID from 1 to 3 mm, and given by

$$N_{\text{conf}} = \frac{\left[\frac{\sigma}{g(\rho_L - \rho_G)}\right]^{0.5}}{D_i}. \tag{23}$$

It is found that Eq. (21) predicts the present data qualitatively well, although it is quantitatively much larger than the present data.

When each experimental run reaches it steady state, the pressure fluctuation in 0.19 mm tube is around 400 Pa, which is about 3–5% of the total pressure loss. On the other hand, that in 0.51 mm tube is about 1960 Pa, which is about 7–12% of the total pressure loss. Therefore, the pressure fluctuation increases as the inner diameter increases. The time period of the fluctuation is about 50–100 s for both cases.

Hetsroni et al. (2003) also measured the pressure fluctuations in their experiments of 210–300 μm triangular microchannels. In their experiments, the pressure fluctuation is about 1500 Pa with a period of 2.5 s. Their pressure fluctuation is about 25–30% of the total pressure loss due to the interaction between parallel microchannels. It is conjectured that the pressure loss fluctuations in a single microtube are much smaller than their device with multiple parallel microchannels.

5. Discussion on heat transfer and pressure loss characteristics in microtubes

It is now clear that the heat transfer characteristics in microtubes are significantly modified, whereas the pressure loss characteristics remain unchanged with considerably lower value. This contradicting fact should be related to the flow patterns in microtubes, and needs to be further discussed.

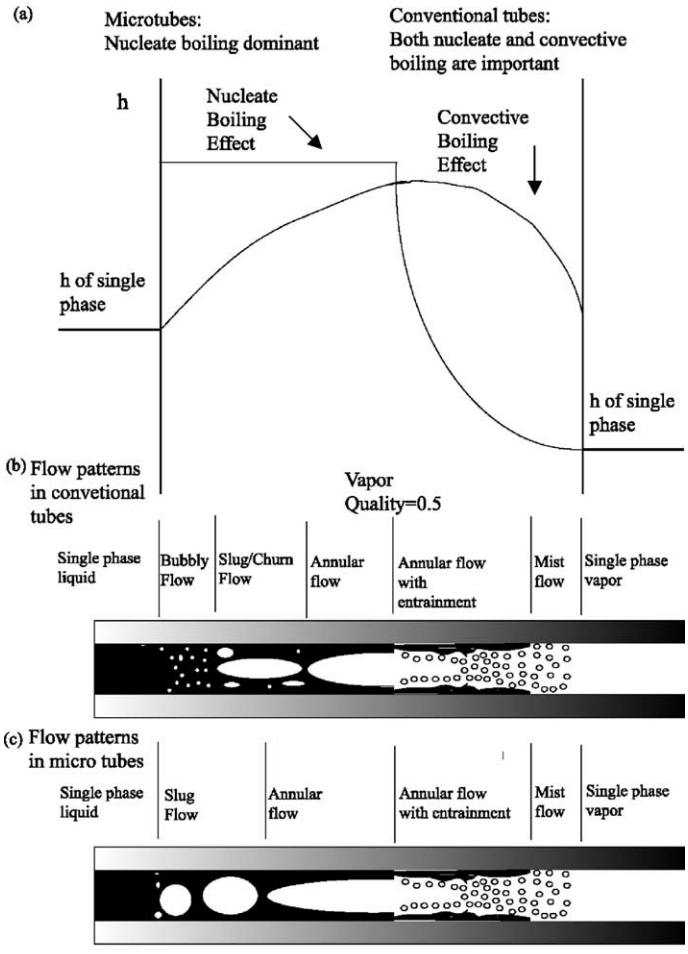

Fig. 24. Schematic of heat transfer coefficient and its relevant flow pattern in conventional tubes and microtubes. (a) Heat transfer coefficient in conventional tubes. (b) Flow patterns in conventional tubes. (c) Flow patterns in microtubes.

Fig. 24(a) and (b) shows the typical distribution of heat transfer coefficient and the associated flow pattern in conventional tubes, deduced from the work of Steiner and Taborek (1992). In conventional tubes, the nucleate boiling effect dominates when the vapor quality is less than 0.5. On the other hand, when the vapor quality exceeds 0.5, the convective boiling effect becomes dominant and the nucleate boiling effect diminishes. As shown in Fig. 22(b), the relevant flow patterns for the nucleate dominant region are the bubbly flow, the churn flow and upstream region of the annular flow, while that for the convective boiling are the downstream region of the annular flow and the mist flow.

In microtubes, however, only annular flow as well as short slug flow regions are discovered (Koo et al., 2000) as shown in Fig. 24(c). As discussed in the previous chapter, the convective boiling effect also diminishes in microtubes. Suppression of both nucleate and convective boiling results in deterioration of the coefficients, which decrease with increasing the vapor quality. In addition, the annular flow remains as a dominant flow pattern and largely contributes to the pressure loss. Therefore, the pressure loss characteristics are qualitatively unchanged in microtubes while their values are much smaller than that predicted by the empirical correlations of Tran et al. (2000).

6. Conclusions

Convective boiling of HCFC123 and FC72 in 0.19, 0.3 and 0.51 mm ID tubes is investigated. The carefully designed temperature measurement and the heat loss compensation make the uncertainty interval of the heat transfer coefficient in the microtubes as low as ±10%. The following conclusions can be derived.

1. Liquid superheat up to 70 K over the saturation temperature is observed at low heat and mass fluxes. The onset of the superheat is found to be dependent on the mass flux and the boiling number for the two different refrigerants examined.
2. In the saturated boiling regime, the heat transfer coefficient is monotonically decreased with increasing the vapor quality, but independent of the mass flux. Most empirical formulas fail to reproduce the present experimental data. The effect of nucleate boiling is found to be dominant, whereas that of the convection boiling should be minor in microtubes.
3. The pressure loss characteristics are found to be qualitatively in accordance with the conventional correlation formula.
4. These contradicting results between the heat transfer and pressure loss characteristics can be explained by the fact that the annular flow prevails in microtubes.

Acknowledgements

The authors are grateful to Mr. Nasu for his aids in the present experiment. The work was supported through the Grant-in-Aid for Scientific Research (No. 13305015) by the Ministry of Education, Culture, Sports, Science and Technology.

References

ANSI/ASME, An American National Standard. Part 1: Measurement Uncertainty. PTC 19.1, 1985.

Bao, Z.Y., Fletcher, D.F., Haynes, B.S., 2000. Flow boiling heat transfer of freon R11 and HCFC123 in narrow passages. Int. J. Heat Mass Transfer 43, 3347–3358.

Bowers, M.B., Mudawar, I., 1994. High flux boiling in low flow rate, low pressure drop mini-channel and microchannel heat sinks. Int. J. Heat Mass Transfer 37, 321–332.

Bjorge, R.W., Hall, G.R., Rohsenow, W.M., 1982. Correlations of forced convective boiling heat transfer data. Int. J. Heat Mass Transfer 25, 753–757.

Brereton, G.J., Crilly, R.J., Spears, J.R., 1998. Nucleation in small capillary tubes. Chem. Phys. 230, 253–265.

Carey, V.P., 1992. Liquid–Vapor Phase-Change Phenomena. Hemisphere Publishing Corporation.

Chen, J.C., 1966. Correlation for boiling heat transfer to saturated fluid in convective flow. I and EC Process Design Dev. 5, 322–329.

Hapke, I., Boye, H., Schmidt, J., 2000. Onset of nucleate boiling in minichannels. Int. J. Therm. Sci. 39, 505–513.

Hetsroni, G., Mosyak, A., Segal, Z., Pogrebnyak, E., 2003. Two-phase flow patterns in parallel micro-channels. Int. J. Multiphase Flow 29, 341–360.

Hsu, Y.Y., 1969. On the size range of active nucleation cavities on a heating surface. Trans ASME: J. Heat Transfer 91, 245–250.

Kandlikar, S.G., 1990. A general correlation for saturated two-phase flow boiling heat transfer inside horizontal and vertical tubes. Trans ASME: J. Heat Transfer 112, 219–228.

Kandlikar, S.G., 2002. Fundamental issues related to flow boiling in minichannels and microchannels. Exp. Therm. Fluid Sci. 26, 389–407.

Kays, W.M., Crawford, M.E., 1993. Convective Heat and Mass Transfer. McGraw Hill.

Kew, P.A., Cornwell, K., 1997. Correlations for the prediction of boiling heat transfer in small-diameter channels. Appl. Therm. Eng. 17, 705–715.

Koo, J. -M., Jiang, L., Zhang, L., Zhou, P., Banerjee, S.S., Kenny, T.W., Santiago, J.G., Goodson, K.E., 2000. Modeling of two phase microchannel heat sinks for VLSI chips. Proc. IEEE. Int. Conf. Micro Electro Mechanical Systems. Miyazaki, pp. 422–427.

Liu, Z., Winterton, R.H.S., 1991. A general correlation for saturated and subcooled flow boiling in tubes and annuli, based on a nucleate pool boiling equation. Int. J. Heat Mass Transfer 34, 2759–2766.

Mehendale, S.S., Jacobi, A.M., Shah, R.K., 2000. Fluid flow and heat transfer at micro- and meso-scales with application to heat exchanger design. Appl. Mech. Rev. 53, 175–193.

Paitoonsurikarn, S., Kasagi, N., Suzuki, Y., 2000. Optimal design of micro bare-tube heat exchanger. Symp. Energy Engineering in the 21st Century, Hong Kong, China, pp. 972–979.

Peng, X.F., Wang, B.-X., 1993. Forced convection and flow boiling heat transfer for liquid flowing through microchannels. Int. J. Heat Mass Transfer 26, 3421–3427.

Ravigururajan, T.S., 1998. Impact of channel geometry on two-phase flow heat transfer characteristics of refrigerants in microchannel heat exchangers. Trans ASME: J. Heat Transfer 120, 485–491.

REFPROP, 1998. Thermodynamic and transport properties of refrigerants and refrigerant mixtures, NIST standard reference database 23, version 6.01.

Saitoh, S., Daiguji, H., Hihara, E., 2000. Boiling heat transfer and pressure drop of HFC134a in horizontal small-diameter tubes. Proc. 39th National Heat Transfer Symp. of Japan, Sapporo, Japan, pp. 667–668.

Schrock, V.E., Grossman, L.M., 1959. Forced convective boiling of water in uniformly heated tubes. Univ. of California, Inst. of Engineering Research, Report no. 73308-UCX-2182, Berkeley, California.

Shah, M.M., 1976. A new correlation for heat transfer during boiling flow through pipes. ASHRAE Trans. 82 (part 2), 66–86.

Steiner, D., Taborek, J., 1992. Flow boiling heat transfer in vertical tubes correlated by an asymptotic model. Heat Transfer Eng. 13, 43–69.

Tran, T.N., Chyu, M.-C., Wambsganss, M.W., France, D.M., 2000. Two phase pressure drop of refrigerants during flow boiling in small channels: an experimental investigation and correlation development. Int. J. Multiphase Flow 26, 1739–1754.

Tuckerman, D.B., Pease, R.F.W., 1981. High-performance heat sinking for VLSI. IEEE Elec. Dev. Lett. EDL-2, 126–129.

Wambsganss, M.W., France, D.M., Jendrzejczyk, J.A., Tran, T.N., 1993. Boiling heat transfer in a horizontal small-diameter tube. Trans ASME: J. Heat Transfer 115, 963–972.

Zhang, L., Wang, E.N., Koo, J. -M., Goodson, K.E., Santiago, J.G., Kenny, T.W., 2002. Enhanced nucleate boiling in microchannels. Proc. IEEE Int. Conf. Micro Electro Mechanical Systems, Las Vegas, USA, pp. 89–92.

Zurcher, O., Thome, J., Favrat, R.D., 1999. Evaporation of ammonia in a smooth horizontal tube: heat transfer measurements and predictions. Trans ASME: J. Heat Transfer. ASME 121, 89–101.